Optical far-infrared properties of a graphene monolayer and multilayer

L. A. Falkovsky[1,2] and S. S. Pershoguba[3,4]
[1]*L.D. Landau Institute for Theoretical Physics, Moscow 117334, Russia*
[2]*Institute of the High Pressure Physics, Troitsk 142190, Russia*
[3]*Moscow Institute of Physics and Technology, Dolgoprudniy 147100, Russia*
[4]*G.V. Kurdyumov Institute for Metal Physics, Kyiv 03142, Ukraine*
(Received 10 July 2007; revised manuscript received 20 September 2007; published 31 October 2007)

We analyze the features of the graphene mono- and multilayer reflectance in the far-infrared region as a function of frequency, temperature, and carrier density taking the intraband conductance and the interband electron absorption into account. The dispersion of plasmon mode of the multilayers is calculated using Maxwell's equations with the influence of retardation included. At low temperatures and high electron densities, the reflectance of multilayers as a function of frequency has the sharp downfall and the subsequent deep well due to the threshold of electron interband absorption and plasmon excitations.

DOI: 10.1103/PhysRevB.76.153410 PACS number(s): 81.05.Uw, 78.67.Ch, 78.67.Pt, 78.66.−w

Monolayer and bilayer graphenes[1–3] are gapless two-dimensional (2D) semiconductors[4–6] whereas its three-dimensional (3D) predecessor, graphite, is a semimetal.[7–9] Hence, the dimensionality effects for the unique substance can be studied.[10] Monolayer graphene has a very simple electron band structure. Near the energy $\varepsilon=0$, the energy bands are cones $\varepsilon_{1,2}(\mathbf{p})=\pm vp$ at the K points in the 2D Brillouin zone with the constant velocity parameter $v=10^8$ cm/s. Such a degeneration is conditioned by symmetry because the small group C_{3v} of the K points has a two-dimensional representation.

While the carrier concentration decreases in the field gate experiment, the graphene conductivity at low temperatures goes to the finite minimal values.[1,2] Much theoretical efforts[11–14] have been devoted to evaluate the minimal conductivity in different approaches. Theoretical[15–17] and experimental researches show that the main mechanism of the carrier relaxation is provided by the charged impurities and gives the collision rate $\tau^{-1}\sim 2\pi^2 e^4 n_{imp}/\hbar\epsilon_g^2\varepsilon$, where ϵ_g is the dielectric constant of graphene, ε is the characteristic electron energy (of the order of the Fermi energy or temperature), and n_{imp} is the density of charged impurities per unit surface. Plasmons in graphene are considered in Refs. 18–20; surface wave propagation along graphene located at interfaces between two dielectrics is studied in Ref. 21. The optical visibility of both monolayer and bilayer graphene is studied in Ref. 22 focusing on the role of the underlying substrate.

In the present Brief Report, we analyze the spectroscopy of the graphene monolayer and multilayers in the infrared region. In order to calculate the reflection coefficient for the multilayers, we follow the method used in Ref. 23 and determine the spectrum of electromagnetic excitations—plasmons. We use the appropriate boundary conditions at interfaces and the complex conductivity σ as a function of frequency ω, temperature T, and chemical potential μ. The chemical potential of ideal pure graphene equals zero at any temperature. With the help of the gate voltage, one can control the density and type (n or p) of carriers varying their chemical potential.

The general expression for the conductivity used here is obtained in our previous paper[18] and is valid under a restriction that the collision rate of carriers is less than the frequency and spatial dispersion of the electric ac field, $\tau^{-1}\ll\omega,kv$. In limiting cases, our result coincides with the formulas of Ref. 24. For high frequencies, when one can also ignore the spatial dispersion of the ac field, $\omega\gg kv,\tau^{-1}$, the complex conductivity [see Eq. (8) in Ref. 18] is given by

$$\sigma(\omega)=\frac{e^2\omega}{i\pi\hbar}\left[\int_{-\infty}^{+\infty}d\varepsilon\frac{|\varepsilon|}{\omega^2}\frac{df_0(\varepsilon)}{d\varepsilon}-\int_0^{+\infty}d\varepsilon\frac{f_0(-\varepsilon)-f_0(\varepsilon)}{(\omega+i\delta)^2-4\varepsilon^2}\right]. \tag{1}$$

Here, the first term corresponds to the intraband electron-photon scattering processes. One can obtain it from the Drude-Boltzmann expression (for a case $1/\tau=0$) and write explicitly

$$\sigma^{intra}(\omega)=i\frac{2e^2T}{\pi\hbar\omega}\ln[2\cosh(\mu/2T)]. \tag{2}$$

The second term in Eq. (1), where $\delta\to 0$ is the infinitesimal quantity determining the bypass around the integrand pole, owes its origin to the direct interband electron transitions. The real part of this contribution is reduced to the expression for the absorbed energy due to the interband transitions. Since there is no gap between the conduction band and valence band, these two terms can compete and the interband contribution becomes larger at high frequencies $\omega>T,\mu$. In the opposite case, the intraband contribution plays the leading role.

The difference of the Fermi functions in the second integrand equals

$$G(\varepsilon)=\frac{\sinh(\varepsilon/T)}{\cosh(\mu/T)+\cosh(\varepsilon/T)}.$$

Extracting the principal value of the integral, we arrive at the integral without singularities and write the interband conductivity in the form available for numerical calculations,

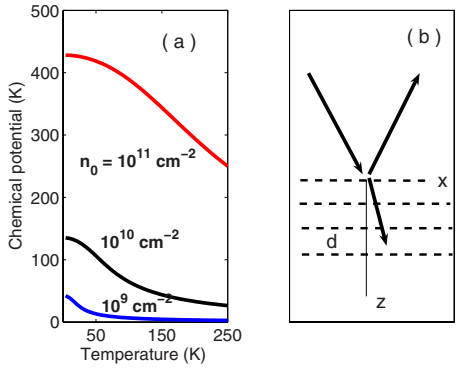

FIG. 1. (Color online) (a) Chemical potential (in K) as a function of temperature at carrier densities noted at curves. (b) Multilayer sample and geometry of wave scattering.

$$\sigma^{inter}(\omega) = \frac{e^2}{4\hbar}\left[G(\omega/2) - \frac{4\omega}{i\pi}\int_0^{+\infty} d\varepsilon \frac{G(\varepsilon) - G(\omega/2)}{\omega^2 - 4\varepsilon^2}\right]. \tag{3}$$

Here, the first term is given asymptotically by

$$G(\omega/2) = \begin{cases} \tanh(\omega/4T), & \mu \ll T \\ \theta(\omega - 2\mu), & \mu \gg T, \end{cases} \tag{4}$$

where the step function $\theta(\omega-2\mu)$ expresses the condition for the interband electron transitions at low temperatures. The integral in Eq. (3) represents the imaginary interband correction to the intraband conductivity. With the help of Eq. (4), we find for low temperatures ($T \ll \mu$)

$$\sigma^{inter}(\omega) = \frac{e^2}{4\hbar}\left[\theta(\omega - 2\mu) - \frac{i}{2\pi}\ln\frac{(\omega+2\mu)^2}{(\omega-2\mu)^2 + (2T)^2}\right]. \tag{5}$$

This expression shows that the interband contribution plays the leading role comparatively with the intraband term around the absorption threshold $\omega \simeq 2\mu$, where the logarithmic singularity is cut off with temperature (or scattering rate while considered).

By using the gate voltage, one can control the density of electrons (n_0) or holes ($-n_0$). Then, the chemical potential is determined by the condition

$$n_0 = \frac{2}{\pi(\hbar v)^2}\int_0^{+\infty} \varepsilon[f_0(\varepsilon - \mu) - f_0(\varepsilon + \mu)]d\varepsilon. \tag{6}$$

From this expression and Fig. 1(a), one can see that the chemical potential goes to zero while the temperature increases.

In order to calculate the graphene reflectance, we apply Maxwell's equations

$$\nabla(\nabla \cdot \mathbf{E}) - \nabla^2\mathbf{E} = \epsilon_0\frac{\omega^2}{c^2}\mathbf{E} + \frac{4\pi i\omega}{c^2}\mathbf{j}, \tag{7}$$

where ϵ_0 is the ion contribution into the dielectric constant and $\mathbf{j}$ is the conductivity current. We consider the case of the p polarization, when the field $\mathbf{E}$ lies in the xz plane and the current $\mathbf{j}$ has only the in-layer x component [see Fig. 1(b)].

(i) *Optics of a monolayer*. Consider the graphene monolayer at $z=0$ with $\epsilon_0 = \epsilon_g$ deposited on the substrate ($z>0$) with the dielectric constant $\epsilon_0 = \epsilon_s$. In the vacuum, $z<0$, the ac field is given by the sum of incident and reflected waves and by the transmitted wave in the substrate. In the geometry considered, the current in the graphene monolayer can be written in the form

$$j_x = \sigma\delta(z)E_x. \tag{8}$$

Making use of the Fourier transformations with respect to the x coordinate, $\mathbf{E} \propto e^{ik_x x}$, we rewrite the Maxwell equations [Eq. (7)] as follows:

$$ik_x\frac{dE_z}{dz} - \frac{d^2E_x}{dz^2} - \epsilon_0\frac{\omega^2}{c^2}E_x = \frac{4\pi i\omega}{c^2}j_x,$$

$$ik_x\frac{dE_x}{dz} + \left(k_x^2 - \epsilon_0\frac{\omega^2}{c^2}\right)E_z = 0. \tag{9}$$

The boundary conditions for these equations at $z=0$ are the continuity of the field component E_x and the jump of the electric-induction z component ϵE_z at the sides of the monolayer,

$$\epsilon_s E_z|_{z=+0} - E_z|_{z=-0} = 4\pi\int_{-0}^{+0}\rho(\omega, k_x, z)dz. \tag{10}$$

The carrier density is connected to the current in Eq. (8) according to the continuity equation

$$\rho(\omega, k_x, z) = j_x(\omega, k_x, z)k_x/\omega.$$

Substituting E_z from the second equation in Eq. (9) into Eq. (10), we find the second boundary condition

$$\frac{\epsilon_s}{k_s^2}\frac{dE_x}{dz}\bigg|_{z=+0} - \frac{1}{(k_z^i)^2}\frac{dE_x}{dz}\bigg|_{z=-0} = \frac{4\pi\sigma(\omega)}{i\omega}E_x\bigg|_{z=0}, \tag{11}$$

where $k_s = \sqrt{\epsilon_s(\omega/c)^2 - k_x^2}$, $k_z^i = \sqrt{(\omega/c)^2 - k_x^2}$.

Using the boundary conditions, we find the reflection amplitude

$$r = \frac{1-C}{1+C}, \tag{12}$$

where $C = k_z^i[4\pi\sigma(\omega)/\omega + (\epsilon_s/k_s)]$.

The reflection coefficient $|r|^2$ calculated with the help of Eqs. (1)–(6) and (12) for normal incidence is shown in Figs. 2 and 3 as a function of frequency, temperature, and carrier concentration. Notice that the carriers have a pronounced (intraband) effect on reflectance only at low frequencies where the dimensionless parameter $e^2\max(T,\mu)/\hbar c\omega$ is of the order of unity. With increasing temperature, the carriers occupy a more expanded energy interval, but the chemical potential decreases. This results in the nonmonotonic behavior of reflectance as a function of temperature shown in Fig. 3.

The optical properties of the graphene bilayer can be considered in a similar way. Here, we do not present the corre-

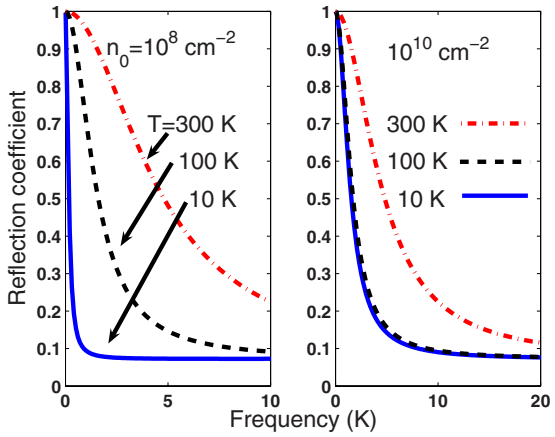

FIG. 2. (Color online) Reflectance from the graphene monolayer with carrier densities $n_0=10^8$ cm^{-2} (left) and $n_0=10^{10}$ cm^{-2} (right) versus the frequency at temperatures noted at the curves: normal incidence.

sponding results, and we investigate another 3D example—the graphene multilayers.

(ii) *Spectroscopy of graphene multilayers*. Let the multilayers cross the z axis at points $z_n=nd$, where d is the distance between the layers [see Fig. 1(b)]. Such a system can be considered as a model of graphite since the distance $d=3$ Å in graphite is larger than the interatomic distance in the layer. So, we describe the carrier interaction in the presence of ac electric field with the help of self-consistent Maxwell's equations [Eq. (7)]. For the x component of the field E_x, they give

$$\left[\frac{d^2}{dz^2}+k_s^2+2k_s\mathcal{D}\sum_n \delta(z-nd)\right]E_x=0, \tag{13}$$

where $\mathcal{D}=2i\pi\sigma(\omega)k_s/\epsilon_g\omega$ and $k_s=\sqrt{\epsilon_g(\omega/c)^2-k_x^2}$.

For the infinite number of layers in the stack, the solutions of Eq. (13) represent two Bloch states

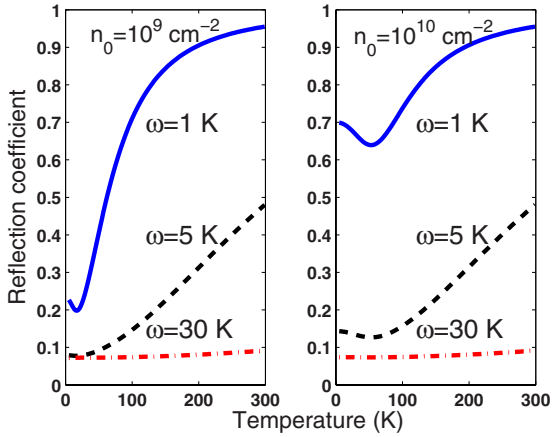

FIG. 3. (Color online) Reflectance from the graphene monolayer with carrier concentrations $n_0=10^9$ cm^{-2} (left) and 10^{10} cm^{-2} (right) versus temperature for frequencies noted at curves: normal incidence.

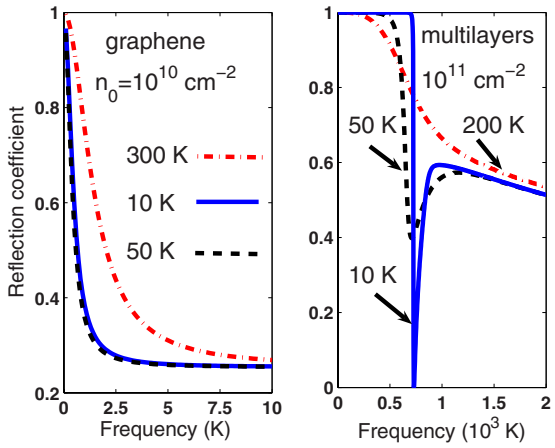

FIG. 4. (Color online) Reflectance from the graphene monolayer with the carrier density $n_0=10^{10}$ cm^{-2} (left) and multilayers with $n_0=10^{11}$ cm^{-2} in a layer and distance $d=3$ Å between layers (right); temperatures are noted at curves and the incidence angle is 80°.

$$e_{1,2}(z)=e^{\pm ik_z nd}\{\sin k_s(z-nd)-e^{\mp ik_z d}\sin k_s[z-(n+1)d]\},$$
$$nd<z<(n+1)d, \tag{14}$$

with the quasimomentum k_z determined from the dispersion equation

$$\cos k_z d=\cos k_s d-\mathcal{D}\sin k_s d. \tag{15}$$

The dispersion equation describes the electric field excitations of the system, i.e., plasmons. The quasimomentum k_z can be restricted to the Brillouin half-zone $0<k_z<\pi/d$, if the parameter $\mathcal{D}$ is real. In the general case, while taking the interband absorption into account, we fix the choice of the eigenfunctions in Eq. (14) by the condition $\mathrm{Im}\,k_z>0$ so that the solution e_1 decreases in the positive direction z. In the long-wave approximation, $k_z,k_s\ll 1/d$, the dispersion equation [Eq. (15)] takes the form

$$\frac{k_z^2}{k_s^2}=1+4\pi i\frac{\sigma(\omega)}{\omega\epsilon_g d}. \tag{16}$$

Reflectance from the multilayers that occupied the semispace $z>0$ can be calculated similarly to the reflectance of a monolayer. The electric field is given by the decreasing solution e_1 inside the sample and by the sum of incident and reflected waves in the vacuum, $z<0$, with the same value of the component k_x.

Using the boundary condition, Eq. (11), with the dielectric constant of graphene ε_g instead of ε_s, we find the reflected amplitude

$$r=\frac{i\sin(k_s d)-Z}{i\sin(k_s d)+Z},$$

where

$$Z=\epsilon_g\frac{k_z^i}{k_s}[\cos(k_s d)-e^{-ik_z d}],$$

k_z^i is the normal component of wave vector in the vacuum, and k_z is the quasimomentum determined by the dispersion

equation [Eq. (15)] at fixed values of ω and k_x.

In Fig. 4, the reflection coefficient calculated for multilayers is shown in comparison with the reflection coefficient of the monolayer. The left panel in this figure differs from the right one in Fig. 2 only in the incidence angle, which is now taken to be 80° in order to emphasize the multilayer features. The main of them is the sharp downfall of reflectance at low temperatures (see the right panel in Fig. 4). This is the threshold effect of the direct interband transitions at $\omega \geqslant 2\mu$, which is sharp when temperature $T \to 0$ [see Eq. (4)]. Just at the downfall, the reflectance has the deep well which disappears while the temperature increases. This is an effect of plasmon excitations. As one can see from Eq. (16), the plasmon excitations with the real k_z are possible if the imaginary part of conductivity is negative. This can be realized if the interband contribution described by the second term in Eq. (5) is larger than the intraband term. Contrary to the monolayer, the peculiarities of reflectance from multilayers take place at larger frequencies $\omega \simeq 2\mu$ because they are governed by the dimensionless parameter $(e^2/\hbar\epsilon_g \mu d)\ln(\mu/k_B T)$, where k_B is the Boltzmann constant. Notice that observations of the absorption threshold provide a direct method of carrier density characterization of graphene $n_0 = (\mu/\hbar v)^2/\pi$.

In conclusion, we have developed the detailed microscopic theory of the graphene mono- and multilayer spectroscopy. We have shown that the nonmonotonic temperature behavior of reflectance from the monolayer in the infrared region is expected. We have argued that at low temperatures and high electron densities, the reflectance from multilayers has the sharp downfall with the subsequent deep well. They are caused by the direct interband electron transitions.

This work was supported by the Russian Foundation for Basic Research (Grant No. 07-02-00571).

[1] K. S. Novoselov, A. K. Geim, S. V. Morozov, D. Jiang, M. J. Katsnelson, I. V. Grigorieva, S. V. Dubonos, and A. A. Firsov, Science **306**, 666 (2004); Nature (London) **438**, 197 (2005).
[2] Y. Zhang, J. P. Small, M. E. S. Amori, and P. Kim, Phys. Rev. Lett. **94**, 176803 (2005); Nature (London) **438**, 201 (2005).
[3] K. S. Novoselov, E. McCann, S. V. Morozov, V. I. Fal'ko, M. J. Katsnelson, U. Zeitler, D. Jiang, F. Shedin, and A. K. Geim, Nat. Phys. **2**, 177 (2006).
[4] M. S. Dresselhaus and G. Dresselhaus, Adv. Phys. **51**, 1 (2002).
[5] N. Ando, J. Phys. Soc. Jpn. **74**, 777 (2005).
[6] E. McCann and V. I. Fal'ko, Phys. Rev. Lett. **96**, 086805 (2006).
[7] P. R. Wallace, Phys. Rev. **71**, 622 (1947).
[8] J. C. Slonczewski and P. R. Weiss, Phys. Rev. **99**, 636(A) (1955).
[9] J. W. MacClure, Phys. Rev. **104**, 666 (1956).
[10] E. Fradkin, Phys. Rev. B **33**, 3263 (1986).
[11] P. A. Lee, Phys. Rev. Lett. **71**, 1887 (1993).
[12] A. W. W. Ludwig, M. P. A. Fisher, R. Shankar, and G. Grinstein, Phys. Rev. B **50**, 7526 (1994).
[13] J. Tworzydlo, B. Trauzettel, M. Titov, A. Rycerz, and C. W. J. Beenakker, Phys. Rev. Lett. **96**, 246802 (2006).
[14] K. Ziegler, Phys. Rev. B **75**, 233407 (2007).
[15] N. Ando, J. Phys. Soc. Jpn. **75**, 074716 (2006).
[16] K. Nomura and A. H. MacDonald, Phys. Rev. Lett. **98**, 076602 (2007).
[17] N. M. R. Peres, F. Guinea, A. H. Castro Neto, Phys. Rev. B **73**, 125411 (2006); J. Nilsson, A. H. Castro Neto, F. Guinea, and N. M. R. Peres, Phys. Rev. Lett. **97**, 266801 (2006).
[18] L. A. Falkovsky and A. A. Varlamov, arXiv:cond-mat/0606800 (unpublished); Eur. Phys. J. B **56**, 281 (2007).
[19] E. H. Hwang and S. Das Sarma, Phys. Rev. B **75**, 205418 (2007).
[20] S. A. Mikhailov and K. Ziegler, Phys. Rev. Lett. **99**, 016803 (2007).
[21] G. W. Hanson, arXiv:cond-mat/0701205 (unpublished).
[22] D. S. L. Abergel, A. Russsell, and V. I. Fal'ko, arXiv:0705.0091 (unpublished).
[23] L. A. Falkovsky and E. G. Mishchenko, JETP Lett. **82**, 96 (2005).
[24] V. P. Gusynin, S. G. Sharapov, and J. P. Carbotte, Phys. Rev. B **75**, 165407 (2007); Phys. Rev. Lett. **96**, 256802 (2006).